Magnetohydrodynamic scenario of plasma detachment in a magnetic nozzle

Alexey V. Arefiev and Boris N. Breizman
Institute for Fusion Studies, The University of Texas, Austin, Texas 78712

(Received 22 July 2004; accepted 20 January 2005; published online 25 March 2005)

Some plasma propulsion concepts rely on a strong magnetic field to guide the plasma flow through the thruster nozzle. The question then arises of how the magnetically confined plasma can detach from the spacecraft. This work presents a magnetohydrodynamic (MHD) detachment scenario in which the plasma flow stretches the magnetic field lines to infinity. Detachment takes place after the energy density of the expanding magnetic field drops below the kinetic energy density of the plasma. As plasma flows along the magnetic field lines, the originally sub-Alfvénic flow becomes super-Alfvénic; this transition is similar to what occurs in the solar wind. In order to describe the detachment quantitatively, the ideal MHD equations have been solved for a cold plasma flow in a slowly diverging nozzle. The solution exhibits a well-behaved transition from sub- to super-Alfvénic flow inside the nozzle and a rarefaction wave at the edge of the outgoing flow. It is shown that efficient detachment is feasible if the nozzle is sufficiently long. © *2005 American Institute of Physics*. [DOI: 10.1063/1.1875632]

I. INTRODUCTION

This work addresses the detachment issue for plasma-based space propulsion systems. Such systems are meant to generate thrust by ejecting directed plasma flow. Some of them employ magnetic nozzles with a strong magnetic field to guide the plasma along the field lines towards the exhaust. The ejected plasma must eventually break-free from the spacecraft in order to produce thrust. The point of concern here is that the field lines from the on-board magnets alone are apparently closed. As a result, the plasma would never be able to fly away from the spacecraft if it moved along *those* lines.

There are two conceivable ways to overcome this difficulty. The first scenario involves breaking the frozen-in constraint, via recombination, or some other mechanism. The second scenario preserves the frozen-in condition. It implies that *plasma detaches from the spacecraft together with the field lines that become stretched along the flow*. The resulting magnetic field in the plume is almost entirely due to the plasma currents. This picture is very similar to what actually happens in the solar wind as it moves away from the Sun.[1]

It is appropriate to accentuate the difference between detachment of plasma and detachment of isolated charged particles. A single ion will readily escape from a magnetic field line if its gyroradius is greater than the characteristic spatial scale of the field. However, for a sufficiently dense plasma, ions can only escape together with electrons to maintain quasineutrality of the plasma. The electrons, which have very small gyroradii, tend to be closely tied to the field lines, and the plasma can remain attached to the magnetic field lines even when the ions themselves are not magnetized. Because of this constraint, it is very difficult to achieve detachment via particle drift motion across the field lines.[2] Plasma recombination in which ions and electrons recombine to form neutrals does not appear to be an attractive detachment mechanism because the recombination rates are typically too low in the expanding nozzle region. The effects of finite resistivity could lead to plasma detachment. However, as concluded in Ref. 3, "the resistive detachment of plasma does not really solve the detachment problem, because the intended thrust will be substantially cancelled by the resistive drag on the plasma by the nozzle magnetic field—no matter what value is achieved by the magnetic Reynolds number." A subsequent study has shown that this conclusion may be too extreme and "plasma detachment can be mediated by several fundamental mechanisms, *all of which are nonideal within the context of magnetohydrodynamics* (MHD)."[4] The above considerations motivate us to investigate the physics of "frozen-in" detachment of plasma from magnetic nozzle, which is the main subject of the paper. In contrast with Ref. 4, we demonstrate that *plasma detachment from the nozzle is possible even within ideal MHD*.

The essence of the frozen-in detachment scenario is delineated in the following quote from Ref. 2. "As the plasma expands down the magnetic field, the ratio of plasma and magnetic field energy densities increases. The ratio of flow energy to magnetic energy is $\beta_f = nM_i u^2/(B^2/\mu_0)$: for flow along constant flux, this ratio is proportional to n^{-1}. As β_f approaches unity, there will be sufficient energy in the plasma for it to tear from the magnetic field. This physics, which includes significant plasma perturbation to the vacuum magnetic field and subsequent reconnection of the field lines, needs to be addressed both *experimentally* and *theoretically*." *Experimental* tests of the described concept in laboratory conditions still remain to be performed. It is the objective of this paper to provide a *theoretical* description of the concept.

The passage of plasma from strong magnetic field region to weak magnetic field region can be viewed as a transition from sub-Alfvénic to super-Alfvénic flow. The important difference between the two is that all the perturbations propagate only downstream in super-Alfvénic flow, whereas, in sub-Alfvénic flow, the perturbations can propagate in both

directions (upstream and downstream). In this respect, a magnetic nozzle is similar to the conventional de Laval nozzle, which transforms subsonic flow into supersonic flow.[5]

A super-Alfvénic plasma flow is guaranteed to detach from the spacecraft. However, the flow directivity may decrease significantly if the super-Alfvénic transition occurs too close to the open end of the nozzle. This raises an immediate question about detachment efficiency, because a strongly diverging plume requires more power than a perfectly directed flow to produce the same thrust.

One of the goals of this paper is to derive the conditions required for efficient super-Alfvénic plasma detachment. In order to do this, we consider a steady-state flow of a cold plasma through a magnetic nozzle that has a perfectly conducting axisymmetric wall to confine a given magnetic flux. It is assumed that the plasma flow inside the nozzle is directed along the magnetic field, whose energy density exceeds the energy density of the flow at the nozzle entrance. We use the ideal magnetohydrodynamics (MHD) model to describe the plasma flow and the magnetic field self-consistently. The problem of plasma detachment can be naturally divided into two subproblems: (1) description of sub- to super-Alfvénic transition inside the nozzle; (2) description of highly super-Alfvénic flow of a cold plasma jet outside the nozzle.

In this paper, for the sake of simplicity, we assume a given flow of a cold plasma at the nozzle entrance and we do not discuss how to create the incoming flow. The specifics of plasma flow formation differ for different thruster concepts. The particular concept that motivated this work is VASIMR (variable specific impulse magnetoplasma rocket).[6] In VASIMR, the plasma flow enters the magnetic nozzle from the ICRH (ion cyclotron resonance heating) module, where the rf power is deposited into the ion gyromotion. The ICRH module creates a flow, in which the ion gyroenergy $m_i v_\perp^2/2$ is much greater than the energy of the axial ion motion $m_i v_\parallel^2/2$ and the spread in $v_\perp$ is relatively small due to a single-pass ICRH scheme.[7] The diverging magnetic field converts the ion rotational motion into the axial motion, accelerating the flow. The acceleration takes place in a strong field that remains unaffected by the plasma flow. After most of the ion gyroenergy is converted into the axial motion, one obtains the required cold plasma flow along the field lines, which we use as an input in our detachment analysis.

The paper is organized in the following way: Sec. II presents a basic equation for the magnetic flux surfaces in a steady-state MHD-flow; Sec. III discusses a particular case of a conical nozzle; Sec. IV contains qualitative analysis of sub- to super-Alfvénic transition in a slowly diverging nozzle and preliminary estimates for nozzle efficiency; and Sec. V describes quantitatively the magnetic field distortion due to plasma flow in the nozzle. This description includes sub- to super-Alfvénic transition. Section VI presents rigorous analysis of the rarefaction wave in the outgoing flow and accurate calculation of the nozzle efficiency. Section VII contains a brief discussion of the results.

II. BASIC EQUATIONS

We start with ideal MHD equations for a steady-state flow of a cold magnetized plasma;[8]

$$\rho(\mathbf{v}\cdot\nabla)\mathbf{v} = -\frac{1}{4\pi}\mathbf{B}\times[\nabla\times\mathbf{B}], \tag{1}$$

$$\nabla\cdot(\rho\mathbf{v}) = 0, \tag{2}$$

$$\nabla\times[\mathbf{v}\times\mathbf{B}] = 0, \tag{3}$$

$$\nabla\cdot\mathbf{B} = 0, \tag{4}$$

where $\mathbf{v}$ is the plasma velocity, ρ is the plasma mass density, and $\mathbf{B}$ is the magnetic field (produced by both, external currents and plasma currents).

We will limit our analysis to the case of a field-aligned flow, in which

$$\mathbf{v} = v\frac{\mathbf{B}}{B}. \tag{5}$$

In such a flow, the magnitude of the plasma velocity v and the ratio ρ/B are constant along the magnetic field lines. Indeed, by taking a scalar product of Eq. (1) with $\mathbf{B}$ and using Eq. (5), we find that

$$\mathbf{B}\cdot\nabla v^2 = 0, \tag{6}$$

after which Eq. (2), with the use of Eqs. (4)–(6), can be rewritten as

$$\mathbf{B}\cdot\nabla\left(\frac{\rho}{B}\right) = 0. \tag{7}$$

We now use Eqs. (5) and (6) to transform Eq. (1) to

$$\frac{\chi}{B}\left(\frac{\mathbf{B}}{B}\cdot\nabla\right)\frac{\mathbf{B}}{B} = -\mathbf{B}\times[\nabla\times\mathbf{B}], \tag{8}$$

with

$$\chi \equiv \frac{4\pi\rho v^2}{B}. \tag{9}$$

As v and ρ/B are constants along the field lines, the quantity χ also does not change along the magnetic field lines. Therefore, the value of χ on each field line is the same as that in the incoming flow.

In what follows, we consider an axisymmetric problem and we use cylindrical coordinates (r,φ,z), with the z axis directed downstream along the axis of symmetry. Moreover, we limit our consideration to the case in which the magnetic field has only r and z components, so that the field can be expressed in terms of a flux function $\Phi(r,z)$:

$$B_r(r,z) = -\frac{1}{r}\left(\frac{\partial\Phi}{\partial z}\right)_r, \tag{10}$$

$$B_z(r,z) = \frac{1}{r}\left(\frac{\partial \Phi}{\partial r}\right)_z. \tag{11}$$

This representation automatically satisfies the condition $\mathrm{div}\,\mathbf{B}=0$. Note that equation $\Phi(r,z)=\mathrm{const}$ specifies an axisymmetric magnetic flux surface.

In view of the fact that χ is a given function of Φ, we change independent variables from r and z to Φ and z. Now r becomes a function of Φ and z, so that

$$dr = \left(\frac{\partial r}{\partial \Phi}\right)_z d\Phi + \left(\frac{\partial r}{\partial z}\right)_\Phi dz. \tag{12}$$

Next, we use Eq. (12) to express the magnetic field components [Eqs. (10) and (11)] in terms of $r(\Phi,z)$:

$$B_r = 2\left(\frac{\partial r}{\partial z}\right)_\Phi \left(\frac{\partial r^2}{\partial \Phi}\right)_z^{-1}, \tag{13}$$

$$B_z = 2\left(\frac{\partial r^2}{\partial \Phi}\right)_z^{-1}. \tag{14}$$

We now transform Eq. (8) to the new variables. Using the vector identity

$$\left(\frac{\mathbf{B}}{B}\cdot\nabla\right)\frac{\mathbf{B}}{B} = -\frac{\mathbf{B}}{B}\times\left[\nabla\times\frac{\mathbf{B}}{B}\right] = -\frac{\mathbf{B}}{B^2}\times\left([\nabla\times\mathbf{B}]+\left[\frac{\mathbf{B}}{B}\times\nabla B\right]\right), \tag{15}$$

we rewrite Eq. (8) in the form

$$\frac{\chi}{B^2}[\mathbf{B}\times[\mathbf{B}\times\nabla B]] = \left(1-\frac{\chi}{B}\right)[\mathbf{B}\times[\nabla\times\mathbf{B}]], \tag{16}$$

where all the terms involving $[\nabla\times\mathbf{B}]$ are collected on the right-hand side. It follows from Eqs. (10) and (11) that $[\nabla\times\mathbf{B}]$ has only a φ component and it is therefore orthogonal to $\mathbf{B}$. Since $[\mathbf{B}\times\nabla B]$ is also orthogonal to $\mathbf{B}$, then Eq. (16) is equivalent to

$$\frac{\chi}{B^2}[\mathbf{B}\times\nabla B] = \left(1-\frac{\chi}{B}\right)[\nabla\times\mathbf{B}]. \tag{17}$$

The only nontrivial component of this equation is its φ component. With the help of Eqs. (10) and (11), we can write down $[\nabla\times\mathbf{B}]_\varphi$ in the following form:

$$\begin{aligned}[\nabla\times\mathbf{B}]_\varphi &= \left(\frac{\partial B_r}{\partial z}\right)_r - \left(\frac{\partial B_z}{\partial r}\right)_z \\ &= \left(\frac{\partial B_r}{\partial z}\right)_\Phi + \left(\frac{\partial B_r}{\partial \Phi}\right)_z\left(\frac{\partial \Phi}{\partial z}\right)_r - \left(\frac{\partial B_z}{\partial \Phi}\right)_z\left(\frac{\partial \Phi}{\partial r}\right)_z \\ &= \left(\frac{\partial B_r}{\partial z}\right)_\Phi - rB_r\left(\frac{\partial B_r}{\partial \Phi}\right)_z - rB_z\left(\frac{\partial B_z}{\partial \Phi}\right)_z \\ &= \left(\frac{\partial B_r}{\partial z}\right)_\Phi - \frac{r}{2}\left(\frac{\partial B^2}{\partial \Phi}\right)_z.\end{aligned} \tag{18}$$

Similarly, we use Eqs. (10) and (11) to calculate $[\mathbf{B}\times\nabla B]_\varphi$:

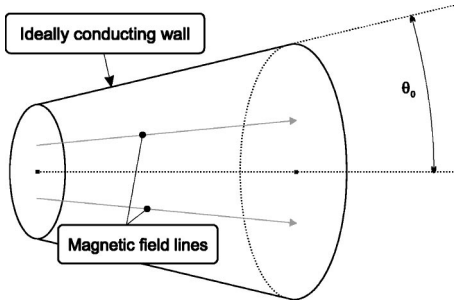

FIG. 1. Magnetic nozzle with a ideally conducting conical wall. The nozzle divergence angle is θ_0.

$$\begin{aligned}[\mathbf{B}\times\nabla B]_\varphi &= B_z\left(\frac{\partial B}{\partial r}\right)_z - B_r\left(\frac{\partial B}{\partial z}\right)_r \\ &= B_z\left(\frac{\partial B}{\partial \Phi}\right)_z\left(\frac{\partial \Phi}{\partial r}\right)_z - B_r\left(\frac{\partial B}{\partial z}\right)_\Phi \\ &\quad - B_r\left(\frac{\partial B}{\partial \Phi}\right)_z\left(\frac{\partial \Phi}{\partial z}\right)_r \\ &= rB^2\left(\frac{\partial B}{\partial \Phi}\right)_z - B_r\left(\frac{\partial B}{\partial z}\right)_\Phi.\end{aligned} \tag{19}$$

Substitution of expressions (18) and (19) into Eq. (17) yields

$$\frac{r}{2}\left(\frac{\partial B^2}{\partial \Phi}\right)_z = \left(\frac{\partial B_r}{\partial z}\right)_\Phi - \left[\frac{\partial}{\partial z}\left(\chi(\Phi)\frac{B_r}{B}\right)\right]_\Phi. \tag{20}$$

This equation, together with Eqs. (13) and (14), determines the form of magnetic flux surfaces $r=r(\Phi,z)$ in a steady-state flow with a given profile of $\chi(\Phi)$. Knowing $r=r(\Phi,z)$, one can find B_r and B_z from Eqs. (13) and (14) and then determine plasma density and flow velocity from Eqs. (5) and (7) using values of ρ and v in the incoming flow.

III. CONICAL NOZZLE

In this section we discuss a particular case of a conical nozzle for which the solution of Eq. (17) can be constructed readily. We consider a nozzle with an infinitely long perfectly conducting wall located at $r(z)=z\tan\theta_0$, where θ_0 is the nozzle divergence angle (see Fig. 1).

In the absence of plasma, the left-hand side of Eq. (17) vanishes and Eq. (17) reduces to $\nabla\times\mathbf{B}=0$. The corresponding vacuum magnetic field is tangential to the nozzle wall at the boundary and has a monopolelike configuration:

$$B_r = \frac{r\Phi_0}{(1-\cos\theta_0)(r^2+z^2)^{3/2}}, \tag{21}$$

$$B_z = \frac{z\Phi_0}{(1-\cos\theta_0)(r^2+z^2)^{3/2}}, \tag{22}$$

where $2\pi\Phi_0$ is the total magnetic flux.

It turns out that the field given by Eqs. (21) and (22) satisfies Eq. (17) even in the presence of plasma, because $[\mathbf{B}\times\nabla B]=0$ for the monopolelike configuration. Therefore, Eqs. (21) and (22) also represent the field in a steady-state plasma flow through the conical nozzle. The magnetic field

and the plasma motion are apparently decoupled in this case. The magnetic field is not affected by the plasma, because there is no plasma current ($\nabla \times \mathbf{B} = 0$). The plasma motion is not affected by the magnetic field, because the field lines are straight.

We now use Eqs. (10) and (11) together with the boundary condition at the perfectly conducting wall,

$$r(\Phi_0, z) = z \tan \theta_0, \tag{23}$$

in order to find $\Phi(r,z)$. By inverting function $\Phi = \Phi(r,z)$, we find that the magnetic flux surfaces are given by

$$r(\Phi, z) = z \sqrt{\left(1 - (1 - \cos \theta_0)\frac{\Phi}{\Phi_0}\right)^{-2} - 1}. \tag{24}$$

The sub- to super-Alfvénic transition is trivial in the case of a conical nozzle, since the plasma motion is free in this case. It is noteworthy that the flow becomes super-Alfvénic without any plasma acceleration. The transition occurs entirely due to the decrease of the magnetic field and the Alfvén velocity downstream. The force-free motion of the plasma is a unique feature of conical nozzle. In a curved guiding magnetic field, the plasma motion and the magnetic field are coupled via plasma currents. It is then important to know whether or not such coupling creates singularities (shock waves) near the super-Alfvénic transition. A favorable answer to this questions is obtained in Secs. IV and V.

IV. PRELIMINARY ESTIMATES AND QUALITATIVE ANALYSIS

In order to estimate the plasma effect on the magnetic field configuration, we consider a paraxial nozzle with a curved ideally conducting wall at $r = R(z)$. The paraxial approximation implies that

$$\theta_0^2 \ll 1, \tag{25}$$

$$\kappa R \ll 1, \tag{26}$$

where $\theta_0 \equiv \partial R / \partial z$ and κ is the field line curvature.

We then estimate the left-hand side of Eq. (20) as

$$\frac{r}{2}\left(\frac{\partial B^2}{\partial \Phi}\right)_z \approx \frac{\delta B}{R}, \tag{27}$$

where δB is the characteristic variation of the magnetic field in the cross section. It is convenient to write down the first term on the right-hand side of Eq. (20) in the following form:

$$\left(\frac{\partial B_r}{\partial z}\right)_\Phi \approx B\left(\frac{\partial}{\partial z}\frac{B_r}{B}\right)_\Phi + \frac{B_r}{B}\left(\frac{\partial B}{\partial z}\right)_\Phi, \tag{28}$$

where

$$B\left(\frac{\partial}{\partial z}\frac{B_r}{B}\right)_\Phi \approx B\frac{\partial \theta_0}{\partial z} \approx \kappa B. \tag{29}$$

We now note that in a paraxial nozzle $BR^2 \approx \text{const}$, so that

$$\frac{B_r}{B}\left(\frac{\partial B}{\partial z}\right)_\Phi \approx B_r R^2 \left(\frac{\partial}{\partial z}\frac{1}{R^2}\right)_\Phi \approx -2\theta_0^2 B. \tag{30}$$

Except for numerical factors, Eqs. (29) and (30) give the following estimate for the first term on the right-hand side of Eq. (20):

$$\left(\frac{\partial B_r}{\partial z}\right)_\Phi \sim \frac{B}{R}(\kappa R + \theta_0^2). \tag{31}$$

The second term on the right-hand side of Eq. (20) can be estimated as

$$\left(\frac{\partial}{\partial z}\left[\frac{4\pi\rho}{B^2}v^2 B_r\right]\right)_\Phi \approx \frac{v^2}{v_A^2}B\left(\frac{\partial}{\partial z}\frac{B_r}{B}\right)_\Phi \approx \frac{v^2}{v_A^2}\kappa B. \tag{32}$$

This estimate takes into account Eq. (9). We now find from Eqs. (20), (31), and (32) that

$$\delta B \sim B\left[\left(1 + \frac{v^2}{v_A^2}\right)\kappa R + \theta_0^2\right]. \tag{33}$$

It follows from Eqs. (33), (25), and (26), that the magnetic field B is nearly constant over the cross section in the absence of plasma flow, i.e.,

$$\delta B \sim B(\kappa R + \theta_0^2) \ll B. \tag{34}$$

The field is also nearly constant in the presence of flow unless the flow is highly super-Alfvénic with

$$v \geqslant \frac{v_A}{\sqrt{\kappa R}}. \tag{35}$$

Equation (33) indicates that, in a slowly diverging paraxial nozzle, the sub- to super-Alfvénic transition does not perturb the magnetic field significantly even if the nozzle is not exactly conical. The corresponding magnetic field distortion can be found with the use of standard perturbative technique (see Sec. V).

As already stated, a super-Alfvénic flow is guaranteed to detach from the nozzle. However, it is important to point out that the flow may somewhat expand and partially lose its directivity in the process of detachment. The expansion is caused by magnetic field pressure that becomes unbalanced when the plasma leaves the nozzle, as the magnetic flux is not confined by the nozzle walls anymore.

In order to explain how the expansion affects the flow, we first review propagation of perturbations in a moving plasma. There is a direct similarity between a supersonic gas flow[9] and a super-Alfvénic plasma flow. If the plasma flow is perturbed at a certain location, the perturbation propagates with the Alfvén speed (relative to the plasma). In addition, the perturbation is also "carried along" by the flow with velocity $\mathbf{v}$. Therefore, a *perturbation* in super-Alfvénic flow *propagates only downstream* within a cone with angle $\theta_A = \sin^{-1}(v_A/v)$.

In the conical nozzle, the flow diverges downstream at an angle θ_0. As a result, perturbation created at the nozzle wall never reaches the axis if θ_0 is bigger than θ_A. Moreover, the smaller the ratio θ_A/θ_0, the smaller the part of the flow affected by the perturbation is (see Fig. 2). If we change the wall configuration, then the plasma flow will change as well.

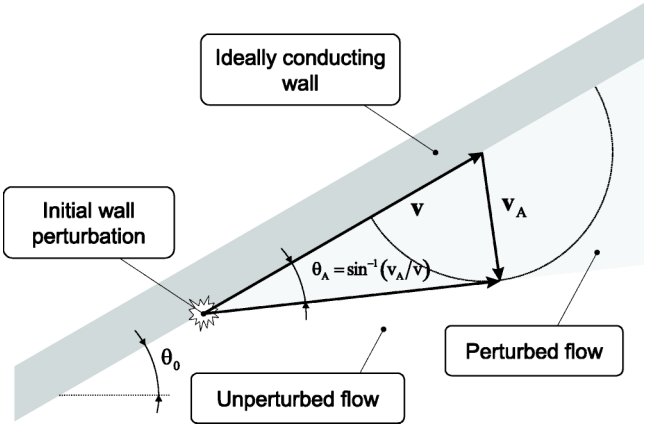

FIG. 2. Perturbations in a super-Alfvénic flow propagate only downstream within a cone with angle $\theta_A=\sin^{-1}(v_A/v)$. If the nozzle divergence angle θ_0 is bigger than θ_A, then a perturbation created at the wall does not propagate inward.

However, the changes involve only a thin layer next to the wall, whereas the rest of the flow is left intact. Clearly, switching from an infinitely long nozzle to a nozzle with an open end can be viewed as a modification of the wall configuration. We thus conclude that, after the strongly super-Alfvénic flow leaves the nozzle, the flow pattern changes only in a thin surface layer of plasma, provided that the nozzle extends sufficiently far downstream ($\theta_0 \gg \theta_A$). Directivity of the main part of the outgoing flow should not be affected in this case.

There are two factors that affect directivity: divergence of the nozzle itself and additional radial expansion of the outgoing flow (plume) at its edge.

In order to estimate the effect of nozzle divergence, we consider an infinitely long nozzle shown in Fig. 3. At the nozzle entrance, the walls are straight and the field lines are parallel to the axis. The nozzle expands slowly and eventually becomes a conical nozzle with angle θ_0.

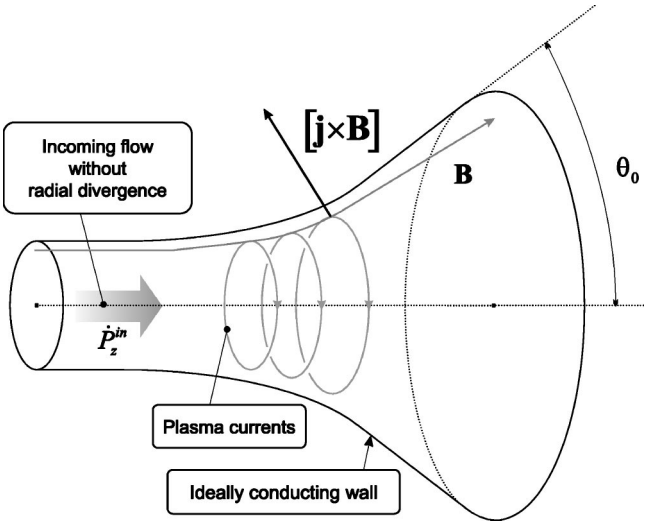

FIG. 3. Nozzle with curved magnetic field lines. At the nozzle entrance, the walls are straight and the field lines are parallel to the axis. The nozzle expands slowly and eventually becomes a conical nozzle with angle θ_0.

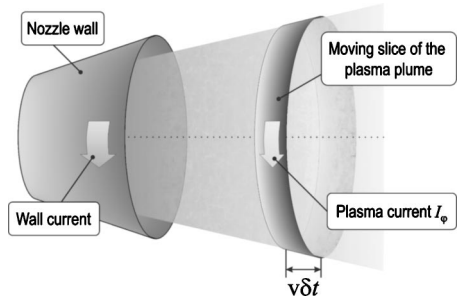

FIG. 4. A moving slice of the plasma plume slows down due to the attraction force between the current in the slice and the wall current.

We introduce nozzle efficiency η as a ratio of the outgoing axial momentum flux $\dot{P}_z^{out}$ to the axial momentum flux in the incoming flow $\dot{P}_z^{in}$:

$$\eta \equiv \frac{\dot{P}_z^{out}}{\dot{P}_z^{in}}. \tag{36}$$

Relative change in axial momentum is $\cos\theta$ for a flux tube that has angle θ with the axis in the conical part of the nozzle. If the flow velocity and plasma density are constant over the cross section of the incoming flow, then the overall efficiency for the paraxial nozzle is given by

$$\eta \approx 1 - \frac{\theta_0^2}{4}. \tag{37}$$

This expression results from straightforward averaging over all flux tubes (see the Appendix for more details).

It is apparent that the axial momentum flux does not change inside the conical part of the nozzle. It only changes in the area where the magnetic field lines curve. Azimuthal plasma currents arise in this area, so that there is a $[\mathbf{j}\times\mathbf{B}]$ force acting on the flow. This force has an axial component directed against the flow (see Fig. 3). In other words, the currents in the nozzle wall attract the plasma currents and this attraction slows down the flow as the plasma proceeds from the cylindrical to conical part of the nozzle.

If the nozzle has a finite length, then the nozzle efficiency will be somewhat reduced by the radial expansion of the plasma. As demonstrated previously, in a highly super-Alfvénic plume, the expansion should affect only a thin outer layer. The magnetic field gradient inside the main part of the flow is much smaller than that inside the layer. Accordingly, the plasma currents are primarily within the outer layer and they have the same direction as the currents in the wall. The wall currents attract the currents in the plume similarly to what happens in the curved part of the nozzle.

To estimate the ensuing decrease in nozzle efficiency,[10] we select a moving slice of the plasma that leaves the nozzle in a time interval δt (see Fig. 4). If the radial thickness of the current layer is Δ, then the plasma current density in the layer is $j_\varphi \approx cB/(4\pi\Delta)$, assuming that the characteristic magnetic field inside the plume B is much larger than the ambient field. Therefore, the total ring current in the selected slice is

$$I_\varphi \approx j_\varphi(v\,\delta t)\Delta \approx \frac{cB}{4\pi} v\,\delta t, \tag{38}$$

where $v\,\delta t$ is the slice thickness.

Apparently, the current in the nozzle wall (per unit length) is $cB/4\pi$. Then the attraction force between the current in the slice and the wall currents is estimated as

$$F_z \sim 2\pi R \frac{I_\varphi}{c}\frac{B}{4}, \tag{39}$$

assuming that the distance between the nozzle opening and the slice is comparable to R.

This force decreases the axial momentum of the slice by

$$\delta P_z \approx F_z \frac{R}{v} \sim \tfrac{1}{8} B^2 R^2 \delta t, \tag{40}$$

as it moves away from the nozzle opening. Here R/v is the time it takes for the slice to move away from the nozzle to the area where the attraction force is negligible.

The momentum of the slice at the nozzle opening is roughly given by

$$P_z \approx v\rho\pi R^2 v\,\delta t, \tag{41}$$

where ρ is the plasma mass density. Then the relative decrease in the axial momentum of the slice is

$$\frac{\delta P_z}{P_z} \sim \frac{B^2 R^2 \delta t}{8\pi v \rho R^2 v\,\delta t} \sim \frac{v_A^2}{2v^2}. \tag{42}$$

We can now combine Eqs. (37) and (42) to estimate the efficiency of a finite length nozzle with a divergence angle θ_0:

$$\eta \sim 1 - \frac{v_A^2}{2v^2} - \frac{\theta_0^2}{4}. \tag{43}$$

It is noteworthy that the inefficiency associated with the plume expansion is insignificant for $\theta_A = v_A/v \ll \theta_0$. This condition requires the nozzle to be sufficiently long.

V. SUB- TO SUPER-ALFVÉNIC TRANSITION IN A PARAXIAL NOZZLE

As shown in the preceding section, the sub- to super-Alfvénic transition has relatively minor effect on the magnetic field profile in a paraxial nozzle. Therefore, the distortion of the magnetic field can be found via a standard perturbation technique.[11] To the lowest order in $\kappa R v^2/v_A^2$ and θ_0, Eq. (20) reads

$$\frac{r}{2}\left(\frac{\partial B^2}{\partial \Phi}\right)_z = 0. \tag{44}$$

This equation shows that the magnetic field is constant in the cross section. The ideally conducting wall confines the magnetic flux radially at $r = R(z)$. The corresponding magnetic flux surfaces inside the nozzle are given by

$$r(\Phi;z) = R(z)\sqrt{\frac{\Phi}{\Phi_0}}. \tag{45}$$

Knowing the lowest order solution, we solve for the first order correction $g(\Phi;z)$, defined as

$$g(\Phi;z) \equiv r^2(\Phi;z) - R^2(z)\frac{\Phi}{\Phi_0}. \tag{46}$$

Equation (20) now becomes an equation for $g(\Phi;z)$:

$$\frac{\partial^2 g}{\partial \Phi^2} = \frac{R^2}{2\Phi_0^2}\left(\frac{\partial R}{\partial z}\right)^2 - \frac{R^5}{4\Phi_0^3}\frac{\partial}{\partial z}\left[\left(\frac{2\Phi_0}{R^2} - \frac{4\pi\rho}{B}v^2\right)\frac{\partial R}{\partial z}\right] \equiv G(\Phi,z). \tag{47}$$

The boundary conditions at the ideally conducting wall and at the axis are

$$g(\Phi_0;z) = 0, \tag{48}$$

$$g(0;z) = 0. \tag{49}$$

The correction satisfying the boundary conditions is given by

$$g(\Phi,z) = \int_0^\Phi ds \int_0^s d\psi G(\psi,z) - \frac{\Phi}{\Phi_0}\int_0^{\Phi_0} ds \int_0^s d\psi G(\psi,z). \tag{50}$$

This expression shows explicitly that the transition from sub-Alfvénic to super-Alfvénic flow is nonsingular if the nozzle is slowly diverging, but not necessarily conical.

VI. RAREFACTION WAVE IN THE OUTGOING FLOW

In this section, we discuss how a highly super-Alfvénic flow continues past the nozzle exit into exhaust. For the sake of simplicity, we assume that the flow velocity and plasma density are constant over the cross section inside the nozzle.

It follows from Eq. (24) that, except for small corrections, the magnetic flux surfaces inside a paraxial nozzle are given by

$$r(\Phi,z) = \theta_0 z\sqrt{\frac{\Phi}{\Phi_0}}, \tag{51}$$

which leads to the following relation between B and z:

$$B = \frac{2\Phi_0}{z^2\theta_0^2}. \tag{52}$$

Prior to describing the rarefaction wave in the plume, we consider small perturbations in a steady-state flow, which result from slight distortion of the conical nozzle.

A. Small perturbations

We define a normalized perturbation of the magnetic flux surfaces as

$$F \equiv \left(r - \theta_0 z\sqrt{\frac{\Phi}{\Phi_0}}\right)\frac{1}{z}\sqrt{\frac{\Phi}{\Phi_0}}. \tag{53}$$

Straightforward linearization of Eq. (20) yields the following equation for the normalized perturbation:

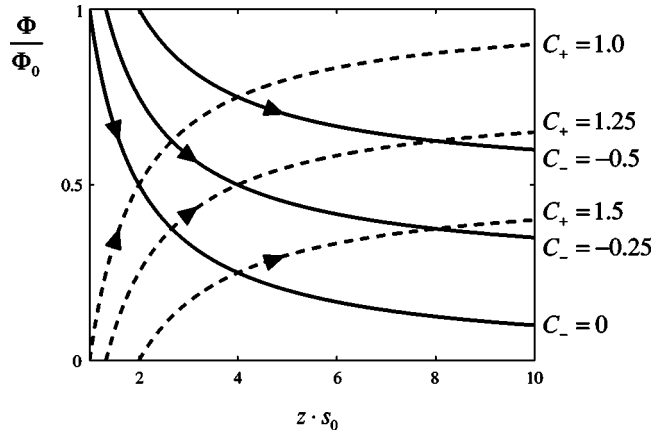

FIG. 5. Characteristics in a highly super-Alfvénic flow. The C_+ characteristics originate at the axis ($\Phi=0$) and the C_- characteristics originate at the wall ($\Phi=\Phi_0$). Quantities Φ and z are normalized to Φ_0 and $1/s_0$, where $2\pi\Phi_0$ is the total magnetic flux and $1/s_0$ is the location of the cutoff point [expression for s_0 is given by Eq. (58)].

$$\frac{8\Phi_0^3}{\theta_0^4}\frac{\Phi}{\Phi_0}\frac{\partial^2 F}{\partial\Phi^2}=\chi_0\frac{\partial^2 F}{\partial s^2}, \tag{54}$$

where

$$s\equiv 1/z \tag{55}$$

and $\chi_0=4\pi\rho v^2/B$ is a parameter independent of z and Φ, which is calculated for the unperturbed quantities inside the nozzle.

Equation (54) is a hyperbolic PDE and it has two families of characteristics,

$$C_+=\left[1-\frac{\Phi}{\Phi_0}\right]+\left[1-\frac{s}{s_0}\right], \tag{56}$$

$$C_-=\left[1-\frac{\Phi}{\Phi_0}\right]-\left[1-\frac{s}{s_0}\right], \tag{57}$$

with

$$s_0\equiv\sqrt{\frac{\theta_0^4\chi_0}{8\Phi_0}}. \tag{58}$$

Similarly to what happens in a steady-state two-dimensional supersonic flow,[12] small perturbations propagate in z along these two families of characteristics. The C_+ characteristics originate at the axis and continue downstream, whereas the C_- characteristics originate at the wall (see Fig. 5).

It follows form Eq. (57) that a C_- characteristic that intersects the wall at $z>z_0=1/s_0$ never reaches the axis. Likewise, a C_+ characteristic, intersecting the axis at $z>z_0=1/s_0$, never reaches the wall. Therefore, $z=z_0$ is a cutoff point, beyond which the wall and the axis "do not communicate." At the cutoff point we have

$$\theta_A(z_0)=\left(\frac{v_A}{v}\right)_{z_0}=\frac{\theta_0}{2} \tag{59}$$

[see Eqs. (58), (52), and (9)]. It is important that only a thin layer of plasma is affected by the distortions of the conical nozzle walls if the distortions occur sufficiently far downstream ($\theta_0\gg\theta_A$).

B. Plume

In this section we construct a rigorous solution for highly super-Alfvénic steady-state plume that consists of two parts: *unperturbed main flow* with straight magnetic field lines and a *rarefaction wave* at the edge of the main flow.

In the case of highly super-Alfvénic flow, Eq. (20) reduces to

$$\frac{r}{2}\left(\frac{\partial B^2}{\partial\Phi}\right)_z=-\chi_0\left(\frac{\partial}{\partial z}\frac{B_r}{B}\right)_\Phi. \tag{60}$$

In the paraxial approximation, the quantities B_r/B and B^2 in this equation are given by

$$\frac{B_r}{B}=2\left(\frac{\partial r}{\partial z}\right)_\Phi, \tag{61}$$

$$B^2=4\left(\frac{\partial r^2}{\partial\Phi}\right)_z^{-2} \tag{62}$$

[see Eqs. (13) and (14)]. We seek the function $r(\Phi;z)$ in the form

$$r(\Phi;z)\equiv zq(\Phi;z), \tag{63}$$

where q is the new unknown function. We also use $s\equiv 1/z$ instead of z as an independent variable. These transformations reduce Eqs. (60)–(62) to the following equation for $q(\Phi;s)$:

$$2q\left[\frac{\partial}{\partial\Phi}\left(\frac{\partial q^2}{\partial\Phi}\right)_s^{-2}\right]_s=-\chi_0\left(\frac{\partial^2 q}{\partial s^2}\right)_\Phi. \tag{64}$$

We will limit our consideration to the case $\theta_0\gg\theta_A$, for which the rarefaction wave is localized at the edge of the plume, where $q\approx\theta_0$ [see Eqs. (51) and (63)]. It is then allowable to replace the multiplier q on the left-hand side of Eq. (64) by θ_0. We now take a Φ derivative of both sides of Eq. (64) to find that

$$2\theta_0\left[\frac{\partial^2}{\partial\Phi^2}\left(\frac{\partial q^2}{\partial\Phi}\right)_s^{-2}\right]_s=-\chi_0\left[\frac{\partial^2}{\partial s^2}\left(\frac{\partial q}{\partial\Phi}\right)_s\right]_\Phi. \tag{65}$$

The magnetic field in the thin outer layer can be approximated by the following expression:

$$B=\frac{1}{r}\left(\frac{\partial r}{\partial\Phi}\right)_z^{-1}\approx\frac{s^2}{\theta_0}\left(\frac{\partial q}{\partial\Phi}\right)_s^{-1}. \tag{66}$$

This allows us to rewrite Eq. (65) as a nonlinear equation for B:

$$\frac{\theta_0^2}{2}\left(\frac{\partial^2}{\partial\Phi^2}\frac{B^2}{s^4}\right)_s=-\chi_0\left(\frac{\partial^2}{\partial s^2}\frac{s^2}{B}\right)_\Phi. \tag{67}$$

The structure of Eq. (67) suggests a separable solution

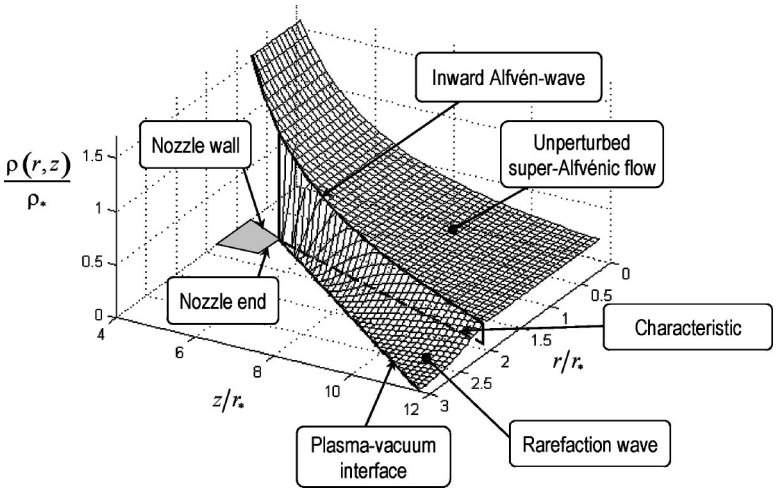

FIG. 6. Two-dimensional plasma density profile in a super-Alfvénic plume.

that is a product of two functions: a function of Φ and a function of s. It can be directly verified that such a solution has the form

$$B = s^2\left(\frac{\chi_0}{\theta_0^2}\right)^{1/3}\left(\frac{\Phi_0-\Phi}{s_*-s}\right)^{2/3}, \tag{68}$$

where s_* is an arbitrary constant.

In order to describe the rarefaction wave, this solution must satisfy two conditions: (1) the magnetic field must vanish at the plume edge, which corresponds to $\Phi=\Phi_0$ and (2) it must match the unperturbed solution (52) on the C_- characteristic that starts at the wall right at the nozzle end. The first condition is apparently satisfied by Eq. (68), whereas the second condition is satisfied if we choose $z_*=1/s_*$ to be the location of the nozzle end. Indeed, the characteristic that corresponds to the boundary between the unperturbed flow and the rarefaction wave is given by

$$1-\frac{\Phi}{\Phi_0}=\sqrt{\frac{8\Phi_0}{\theta_0^4\chi_0}}(s_*-s). \tag{69}$$

Substitution of this expression into Eq. (68) yields the unperturbed field given by Eq. (52).

Equation (68) gives magnetic field in the rarefaction wave in terms of Φ and s. In order to find $B=B(r,z)$, we have to find $r=r(\Phi,z)$ first. Taking into account that $\partial r/\partial z$ is continuous at the C_- characteristic and using Eqs. (53), (63), (66), and (68), we obtain

$$r(\Phi;z)=z\theta_0+2z\left[1-\frac{z_*}{z}\right]\frac{v_A}{v}-3z\left[\frac{\theta_0}{2}\frac{v_A^2}{v^2}\right]^{1/3}\times\left[1-\frac{z_*}{z}\right]^{2/3}\left[1-\frac{\Phi}{\Phi_0}\right]^{1/3}, \tag{70}$$

where v_A is calculated for the unperturbed magnetic field and plasma density at the nozzle end. Finally, Eq. (68) together with Eq. (70) yields

$$B(r,z)=B_*\frac{z_*^2}{z^2}\frac{v^2}{9v_A^2}\times\left[1-\frac{z_*}{z}\right]^{-2}\left[\frac{r}{z}-\theta_0-\frac{2v_A}{v}\left(1-\frac{z_*}{z}\right)\right]^2, \tag{71}$$

where B_* is the magnetic field at the nozzle opening.

In order to find plasma density in the plume we use the fact that the ratio ρ/B is constant along the magnetic field lines, so that ρ has the same spatial dependence as B. The corresponding plasma density profile is shown in Fig. 6. The location of the plasma-vacuum interface ($\Phi=\Phi_0$) follows directly from Eq. (70):

$$r_{pv}=z\theta_0+2z\left[1-\frac{z_*}{z}\right]\frac{v_A}{v}. \tag{72}$$

The inner boundary of the layer is located at

$$r_c=z\theta_0\sqrt{1-\frac{2}{\theta_0}\frac{v_A}{v}\left(1-\frac{z_*}{z}\right)}, \tag{73}$$

which follows from Eqs. (51) and (69).

It is important to point out that for $z\gg z_*$, Eqs. (72) and (73) reduce to

$$r_{pv}\approx(\theta_0+2\theta_A)z, \tag{74}$$

$$r_c\approx(\theta_0-\theta_A)z, \tag{75}$$

which means that the magnetic field lines become straight asymptotically. As the momentum flux in such a flow remains constant, the asymptotic flow is completely detached from the nozzle.

To conclude this section, we give the complete expression for the magnetic field in the plume:

$$B(r;z)=\begin{cases}\dfrac{2\Phi_0}{z^2\theta_0^2}, & r\leqslant r_c\\ B_*\dfrac{z_*^2}{z^2}\dfrac{v^2}{9v_A^2}\left[1-\dfrac{z_*}{z}\right]^{-2}\left[\dfrac{r}{z}-\theta_0-\dfrac{2v_A}{v}\left(1-\dfrac{z_*}{z}\right)\right]^2, & r_c<r<r_{pv}\\ 0, & r_{pv}\leqslant r,\end{cases} \tag{76}$$

where z_* is the location of the nozzle end, B_* is the magnetic field at the nozzle end, and v_A is the Alfvén speed calculated for the unperturbed magnetic field and plasma density at the nozzle end. The quantities r_c and r_{pv} are defined as

$$r_c=z\theta_0\sqrt{1-\frac{2}{\theta_0}\frac{v_A}{v}\left(1-\frac{z_*}{z}\right)}, \tag{77}$$

$$r_{pv}=z\theta_0+2z\left[1-\frac{z_*}{z}\right]\frac{v_A}{v}. \tag{78}$$

VII. SUMMARY AND DISCUSSION

We have demonstrated that a slowly diverging nozzle provides well-controlled transition from sub- to super-Alfvénic plasma flow. The transition occurs without any significant perturbation of the guiding magnetic field. The super-Alfvénic flow detaches from the nozzle at the nozzle end, with the nozzle efficiency roughly given by

$$\eta\sim 1-\frac{\theta_0^2}{4}-\frac{v_A^2}{2v^2}, \tag{79}$$

where θ_0 is the nozzle divergence angle and v_A is the Alfvén speed calculated for the unperturbed magnetic field and plasma density at the nozzle end. The inefficiency associated with the detachment is insignificant for $v_A/v\ll\theta_0$. This inequality requires the nozzle to be sufficiently long. In the paraxial case, reconnection events (if any) can only occur in the super-Alfvénic plume outside the nozzle, so that the flow inside the nozzle is unaffected. The effect of reconnection on detachment efficiency should then be minimal.

In this work, consideration is limited to steady-state plasma flow. A time-dependent simulation is required in order to understand how the steady-state regime establishes. Such simulations would also allow to quantify the effect of transient phenomena on the nozzle efficiency.

Another natural extension of the presented work would be a stability analysis of the described flow. It is apparent that low-frequency MHD instabilities are very likely to be suppressed, because the ion lifetime in the magnetic nozzle is extremely short. What is less clear is the role of higher frequency instabilities that may break the frozen-in condition due to anomalous resistivity. Also, strong velocity shear inside the nozzle may be unstable.

Our description of the rarefaction wave in the outgoing flow (Sec. VI) implies that there is no vacuum gap between the plasma and the nozzle wall. In reality, the vacuum gap with magnetic field in it may actually be present. If this is the case, then for highly super-Alfvénic flow, the plume will still consist of two distinct parts: unperturbed main flow with straight magnetic field lines and a rarefaction wave at the edge of the main flow. The presence of the magnetic field in the vacuum gap affects only the thin outer layer associated with the rarefaction wave. The magnetic field that comes out of the gap decreases away from the opening at a distance comparable to the width of the gap. Even if the width of the gap is comparable to the radius of the nozzle, the rarefaction wave is not expected to change the nozzle efficiency significantly for highly super-Alfvénic flow.

If the plasma density drops towards the nozzle wall, then there may exist a thin sub-Alfvénic boundary layer near the wall. The super-Alfvénic part of the flow will detach from the spacecraft after leaving the nozzle, whereas the sub-Alfvénic layer may not be able to escape. Even though this thin outer layer carries only a small fraction of the plasma, there is a concern about spacecraft surface damage by the layer plasma. Absorbing limiters may be needed to deal with this issue.

In conclusion, we note that experimental verification of the super-Alfvénic detachment concept in laboratory appears to be feasible. For example, the gas-dynamic trap,[13] an axisymmetric mirror machine with large mirror ratio, is particularly suitable for such an experiment.

ACKNOWLEDGMENTS

This work was supported by the VASIMR Plasma Thruster project at NASA and by the U.S. Department of Energy under Contract No. DE-FG03-96ER-54346. The authors thank Dr. Roger Bengtson, Dr. Franklin Chang-Dìaz, Dr. Dmitri Ryutov, and Dr. Roald Sagdeev for stimulating discussions.

APPENDIX: NOZZLE EFFICIENCY

As defined by Eq. (36) in Sec. IV, the nozzle efficiency is the ratio of the axial momentum flux in the outgoing flow at $z\rightarrow+\infty$ to the axial momentum flux in the incoming flow.

For the plume described in Sec. VI B, the axial momentum flux in the outgoing flow

$$\dot{P}_z^{out}=\left[\int_0^\infty \rho v_z^2 2\pi r dr\right]_{z\rightarrow+\infty} \tag{A1}$$

is equal to the surface integral of the stress-tensor over the nozzle outlet,

$$\dot{P}_z^{out} = \left[\int_0^{r_0} \Pi_{zz} 2\pi r dr \right]_{z=z_*}, \tag{A2}$$

where z_* is the location of the outlet, r_0 is its radius, and the stress-tensor is defined as

$$\Pi_{ik} = \rho v_i v_k - \frac{1}{4\pi}\left(B_i B_k - \frac{1}{2} B^2 \delta_{ik} \right). \tag{A3}$$

Note that, in general, the upper limit of integration in Eq. (A2) should extend to infinity. However, it follows from Sec. VI B that there is no magnetic field outside the plume (within the validity range of the ideal MHD description), so that the integral from r_0 to infinity gives no contribution to Eq. (A2). It must be pointed out that the frozen-in condition may breakdown at the plume edge, where the plasma density becomes very low. This would allow a small portion of the magnetic flux to leave the plume and produce a corresponding contribution to Π_{zz} at $r > r_0$. In order to find the resulting correction to nozzle efficiency, one has to go beyond the ideal MHD model presented in this paper.

The equivalence of expressions (A1) and (A2) is a consequence of the momentum flux conservation in a steady-state flow,

$$\nabla_k \Pi_{ik} = 0. \tag{A4}$$

Indeed, it follows from Eq. (A4) that the surface integral in Eq. (A2) is equal to the surface integral of Π_{zz} over the plume cross section at $z = +\infty$. The magnetic field contribution to the integral vanishes as $z \to +\infty$, so that it is equal to the expression given by Eq. (A1) and, therefore, Eqs. (A1) and (A2) are equivalent.

The axial momentum flux in the incoming flow can also be expressed in terms of the flow density and velocity at the nozzle outlet:

$$\dot{P}_z^{in} = \left[\int_0^{r_0} (\rho v_z v) 2\pi r dr \right]_{z=z_*}. \tag{A5}$$

In order to obtain Eq. (A5), we consider a thin coaxial flux tube with the inner radius r and outer radius $r+dr$ at the outlet. The mass flux through the tube is $(\rho v_z)_{z_*} 2\pi r dr$, which is constant along the flux tube. The momentum flux through the tube in the incoming flow without radial divergence is $(\rho v_z v)_{z_*} 2\pi r dr$, where we took into account that the flow velocity v is constant along the tube. Integration over all the flux tubes gives Eq. (A5).

We now use Eqs. (A2) and (A5) to find that the nozzle efficiency is

$$\eta = \frac{\dot{P}_z^{out}}{\dot{P}_z^{in}} \approx \left[\frac{\int_0^{r_0} (\rho v_z^2 - B_z^2/8\pi) r dr}{\int_0^{r_0} (\rho v_z v) r dr} \right]_{r=r_*}, \tag{A6}$$

where the B_r^2 term was neglected, because $B_z \gg B_r$. The axial component of the flow velocity can be written as $v_z = v \cos\theta \approx v(1-\theta^2/2)$, where $\theta = \theta(r)$ is the angle between the flux tube and the axis. This allows us to reduce Eq. (A6) to

$$\begin{aligned} \eta &\approx 1 - \left[\frac{\int_0^{r_0} (\rho v_z v \theta^2/2 + B_z^2/8\pi) r dr}{\int_0^{r_0} \rho v_z v r dr} \right]_{r=r_*} \\ &\approx 1 - \left[\frac{\int_0^{r_0} (\rho v^2 \theta^2/2 + B_z^2/8\pi) r dr}{\int_0^{r_0} \rho v^2 r dr} \right]_{r=r_*}. \end{aligned} \tag{A7}$$

Finally, we evaluate the integrals in Eq. (A7) for a straight conical nozzle with $\theta \approx r/z_*$ and uniform flow velocity and density in the cross-section $[v(r,z_*) = v, \rho(r,z_*) = \rho_*]$ to find that

$$\eta \approx 1 - \frac{\rho_* v^2 r_0^2 \theta_0^2/4 + B_*^2 r_0^2/8\pi}{\rho_* v^2 r_0^2} \approx 1 - \frac{\theta_0^2}{4} - \frac{v_A^2}{2v^2}, \tag{A8}$$

where $\theta_0 \equiv r_0/z_*$, $v_A \equiv B_*/\sqrt{4\pi\rho_*}$, and $B_* \equiv B_z(0, z_*)$.

[1] E. N. Parker, Astrophys. J. **128**, 664 (1958).
[2] E. B. Hooper, J. Propul. Power **9**, 757 (1993).
[3] R. A. Gerwin, G. J. Marklin, A. G. Sgro, and A. H. Glasser, LANL Technical Report No. AL-TR-89-092 (unpublished).
[4] R. W. Moses, Jr., R. A. Gerwin, and K. F. Schoenberg, Space Nuclear Power Systems, edited by Mohamed S. El-Genk and Mark D. Hoover, AIP Conf. Proc. 246 (AIP, New York, 1992), p. 1293.
[5] L. D. Landau and E. M. Lifshitz, *Fluid Mechanics*, 2nd ed. (Pergamon, Oxford, 1979), p. 348.
[6] F. R. Chang-Dìaz, Sci. Am. **283**, 90 (2000).
[7] A. V. Arefiev and B. N. Breizman, Phys. Plasmas **11**, 2942 (2004).
[8] L. D. Landau and E. M. Lifshitz, *Electrodynamics of Continuous Media*, 2nd ed. (Pergamon, Oxford, 1984), p. 225.
[9] L. D. Landau and E. M. Lifshitz, *Fluid Mechanics*, 2nd ed. (Pergamon, Oxford, 1979), p. 310.
[10] A formal calculation of the nozzle efficiency is given in the Appendix. In our subsequent qualitative estimates [Eqs. (38)–(43)], which are only good to within numerical factors, we adjust the coefficients to make the results consistent with the Appendix.
[11] V. P. Nagornyj, D. D. Ryutov, and G. V. Stupakov, Nucl. Fusion **24**, 1421 (1984).
[12] L. D. Landau and E. M. Lifshitz, *Fluid Mechanics*, 2nd ed. (Pergamon, Oxford, 1979), p. 433.
[13] A. A. Ivanov, A. V. Anikeev, P. A. Bagryansky, P. P. Deichuli, S. A. Korepanov, A. A. Lizunov, V. V. Maximov, S. V. Murakhtin, V. Ya. Savkin, D. J. Den Hartog, G. Fiksel, and K. Noack, Phys. Rev. Lett. **90**, 105002 (2003).